Philosophical Magazine,
Vol. 85, No. 25, 1 September 2005, 2947–2960

Taylor & Francis
Taylor & Francis Group

Local structure of technologically modified g-GeS_2: resonant Raman and absorption edge spectroscopy combined with *ab initio* calculations

R. HOLOMB*†, P. JOHANSSON‡, V. MITSA† and I. ROSOLA†

†Uzhgorod National University, Department of Solid State Electronics,
54 Voloshyn Str., Uzhgorod 88000, Ukraine
‡Chalmers University of Technology, Department of Applied Physics,
Göteborg 41296, Sweden

(*Received 22 February 2005; in final form 23 March 2005*)

We have used resonant Raman and absorption edge spectroscopy together with first-principle calculations in order to study the structure of GeS_2 glasses (g-GeS_2). The glasses were prepared under different melt temperatures and cooling rates, which are shown to significantly influence the g-GeS_2 structure at the nano-scale. The combined use of Raman spectroscopy and *ab initio* calculations reveals the origin of the molecular level electronic structure and its connection to the interesting technological features of the g-GeS_2. Local structure within the glasses is discussed in terms of atomic Ge_nS_m clusters. The band gaps computed for these clusters and their correlation to the experimental band gaps and the possible formation of band tail states are also discussed.

1. Introduction

The structure and its coupling to the fundamental physical properties of amorphous (a) and/or glassy (g) materials has been the subject of intensive studies for many years [1]. The considerable attention on chalcogenide glasses (based on S, Se, or Te) is mainly due to their foreseen practical usage possibilities. It is known that chalcogenide materials can be used as a sensitive media for optical recording (CD, CDRW, DVD), useful optoelectronic elements, laser-technology devices, light guides, and anti-reflecting coatings [2]. Moreover, bulk GeS_2 glasses (g-GeS_2) with Ag^+ cations are solid electrolytes with a high ionic conductivity at room temperature [3]. The structure and physical properties of g-GeS_2 have been investigated previously using both experimental [4–8] and theoretical [7, 9–11] approaches. However, the interpretation of experimental results to determine basic structural units at nano-scale is difficult due to the absence of unambiguous experimental techniques for the investigation of medium-range order in amorphous structures. However, several recent studies [7, 11, 12] show agreement between experimental data and computer simulations of glass structure and properties. In this work this approach

*Corresponding author. Email: holomb@ukr.net

Philosophical Magazine
ISSN 1478–6435 print/ISSN 1478–6443 online
http://www.tandf.co.uk/journals
DOI: 10.1080/14786430500156112

is applied to g-GeS_2 by employing spectroscopic experimental techniques and *ab initio* calculations. Ultimately, computational methods can be used not only for a detailed interpretation of performed experiments, but also to predict the properties of amorphous materials.

For the local structure and bond order in a glassy network the preparation conditions are important. In return, the resulting local structural peculiarities (*e.g.* dangling bonds, defects, interstitial atoms) in chalcogenide glasses can produce localized electronic states: band tail states — on top of the valence band and on bottom of the conduction band [8, 13]. These band tail states have vast influence on the optoelectronic properties of the materials and can thus be tailored by using different technological conditions of glass preparation.

In this work, resonant Raman and absorption edge spectroscopy together with *ab initio* calculations have been used to elucidate the local structure and resulting band gaps of g-GeS_2 prepared under different conditions.

2. Experimental and theoretical details

2.1. *Sample preparation and experimental methods*

The g-GeS_2 samples were synthesized by melt quenching from different temperatures ranging from 1173 K (T_1) to 1473 K (T_4) and cooling rate variations from 100 K/s (V_1) to 150 K/s (V_2). The four different g-GeS_2 samples will hereafter be denoted (T_1, V_1), (T_2, V_2), (T_3, V_2), and (T_4, V_2). The synthesis of crystalline GeS (c-GeS) is described elsewhere [14, 15].

Raman spectra of g-GeS_2 and c-GeS were measured using Dilor–Labram and Renishaw system 1000 Raman spectrometers equipped with CCD detectors. The laser sources used for Raman scattering excitation of g-GeS_2 were as follows: (i) a diode laser (785 nm), (ii) a He–Ne laser (632.8 nm), and (iii) an Ar-ion laser (514.5 and 488 nm). Optical filters, limiting the output power, were used in order to avoid photostructural changes of the materials. The spectra were measured in micro-Raman configuration using a back-scattering geometry. The Raman spectrum of c-GeS was measured using a Spectra Physics Model 168 Ar-ion laser (514.5 nm, 1 W).

Absorption spectra of g-GeS_2 were measured at 80 and 293 K using an SF-46 spectro-photometer. A standard method based on the analysis of light transmission and reflection was used. The glasses were sliced and polished to produce high-quality sample surfaces. The sample thicknesses were chosen to provide the maximum accuracy of absorption edge measurements within the α range of interest.

2.2. *Calculational methods*

The computational part consists of first-principle calculations on small atomic Ge_nS_m clusters ($1 < n < 3, 1 < m < 9$) as depicted in figure 1. All clusters were suitably terminated by use of hydrogen atoms.

Initial calculations were performed using the Gaussian-03 quantum-chemical program package [16]. The self-consistent field (SCF) and Hartree–Fock (HF) methods were applied for geometry optimizations of the clusters using the

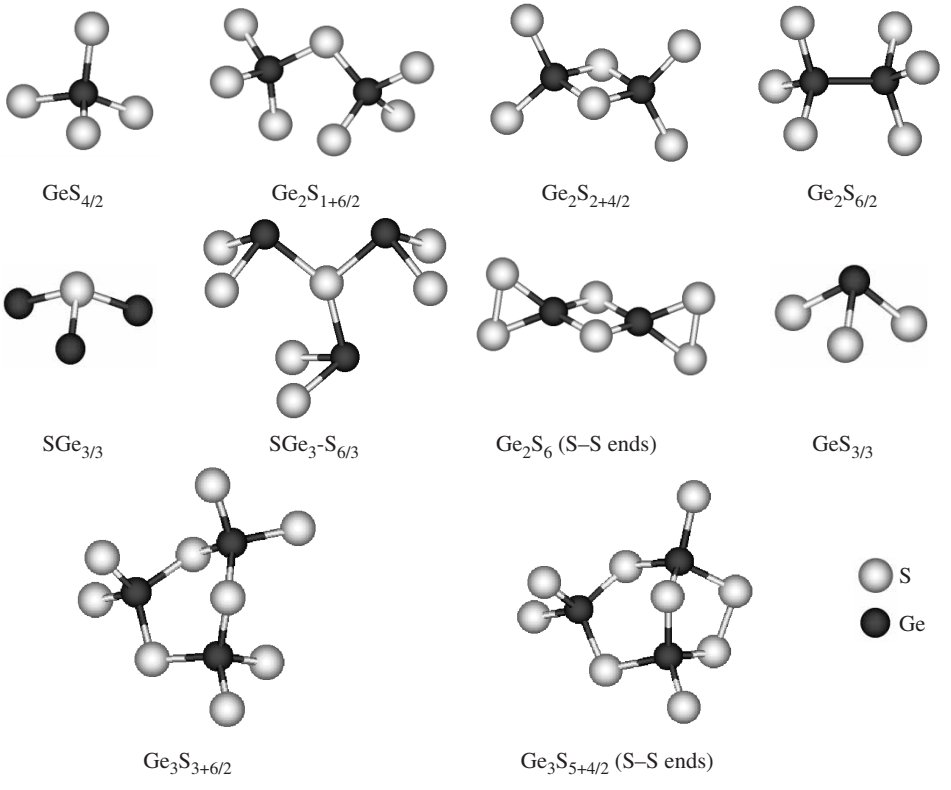

Figure 1. The structural models of Ge_nS_m clusters used for ab initio calculations of vibrational spectra: single tetrahedra ($GeS_{4/2}$); corner-shared bi-tetrahedra ($Ge_2S_{1+6/2}$); edge-shared bi-tetrahedra ($Ge_2S_{2+4/2}$); edge-shared bi-tetrahedra closed by S–S ends (Ge_2S_6); ethane-like cluster ($Ge_2S_{6/2}$); three-fold coordinated structures ($SGe_{3/3}$, SGe_3–$S_{6/3}$, $GeS_{3/3}$); fragment of c-GeS_2 ring ($Ge_3S_{3+6/2}$) and a model of the Phillips "outrigger raft" ($Ge_3S_{5+4/2}$). Saturating hydrogen atoms and corresponding bonds are not shown for clarity.

Berny optimization procedure. The triple zeta valence Pople 6-311G* [17] basis set was used for the Ge and S atoms. For the H atoms the 3-21G basis set was used. Subsequent second derivative calculations, using the same method and basis set, verified the obtained structures as true energy minimum geometries. In order to eliminate the influence of the hydrogen atoms in the Raman spectra calculations the GAMESS (US) software was used [18]. The algorithm of elimination is described elsewhere [19].

While the HF approximation is very useful to provide basic structural data, it also has severe shortcomings (*e.g.* incorrect bond dissociation). As a result too high vibrational frequencies are obtained and this cannot be totally corrected for by using larger basis sets [20]. However, by assuming that the error is constant for all vibrations, or at least for a group of vibrations having similar force constants, a linear scaling factor can be used. Here an empiric factor of 0.94 was used to scale the frequencies calculated at the HF/6-311G* level of theory.

In order to increase the accuracy of the HF calculations either "post-HF" methods or methods based on density functional theory (DFT) can be used, primarily to account for electron correlation. Here we applied DFT methods to obtain more accurate band gaps. The basis sets used were the same as for the HF calculations and used together with the corrected exchange functional proposed by Becke [21] and the gradient-corrected correlation functional of Lee *et al.* [22] (BLYP). The band gaps were estimated in two different ways. The simplest approximation used was the energy difference between the HOMO and LUMO molecular orbital energies (ΔE_{g1}) [23]. However, the LUMO is a virtual-type orbital connected only with the ground-state. Therefore, in addition, the low-lying excited states of the clusters were calculated using a time dependent (TD) approach (TD-DFT) (ΔE_{g2}) [24].

3. Results

3.1. *Experimental Raman spectra of g-GeS_2*

In figure 2 the resulting Raman spectra of g-GeS_2 was measured using a photon energy of 2.42 eV (514.5 nm), less than the Tauc optical gap of GeS_2 glasses ($E_g \sim 3.2$ eV) [14] that are shown. As these spectra are similar to those measured with longer wavelengths: 632.8 and 785 nm, corresponding to 2.41 and 1.58 eV (not shown), we assign these to be non-resonant Raman spectra. All spectra are normalized using the 342 cm^{-1} peaks. A pronounced difference between the samples is that both the (T_1, V_1) and the (T_3, V_2) samples show similar small increases in the 370 and 433 cm^{-1} vibrational modes, as compared to (T_2, V_2), and for the (T_4, V_2) sample these peaks broaden and merge with the main peak at 342 cm^{-1}. A very weak mode at $\sim$200 cm^{-1} is observed for all samples while a weak Raman mode at 490 cm^{-1} is detected only for (T_2, V_2). The most pronounced differences, however, occur at the low frequency side of the main peak: new peaks arise at 256 and 237 cm^{-1}, especially strong for (T_4, V_2). Polarized Raman spectra of single crystal c-GeS are shown in the insert of figure 2.

To examine the influence of photon energy on intensities of Raman modes (*i.e.* possible resonance Raman features) the (T_1, V_1), (T_2, V_2), and (T_3, V_2) samples were excited as above by a 514.5 nm laser (2.42 eV) and in addition with a shorter wavelength (blue) laser of 488 nm, increasing the photon energy to 2.54 eV. The resulting spectra for (T_1, V_1) and (T_2, V_2) are shown in figure 3 and intensity increases for the two Raman modes at 370 and 433 cm^{-1} which are observed for both samples. All intensities were taken as peak height values. Figure 4 shows the intensity ratios of the 370 and 433 cm^{-1} modes as compared with the intensity of the main mode at 342 cm^{-1}, (I_{370}/I_{342}) and (I_{433}/I_{342}), respectively, as functions of excitation photon energy, and shows clearly the mainly common behaviour of the glasses.

3.2. *Computed local structures, Raman spectra, and band gaps of g-GeS_2*

Calculated and scaled vibrational frequencies for the Ge_nS_m clusters (figure 1) and the corresponding Raman intensities are tabulated in table 1.

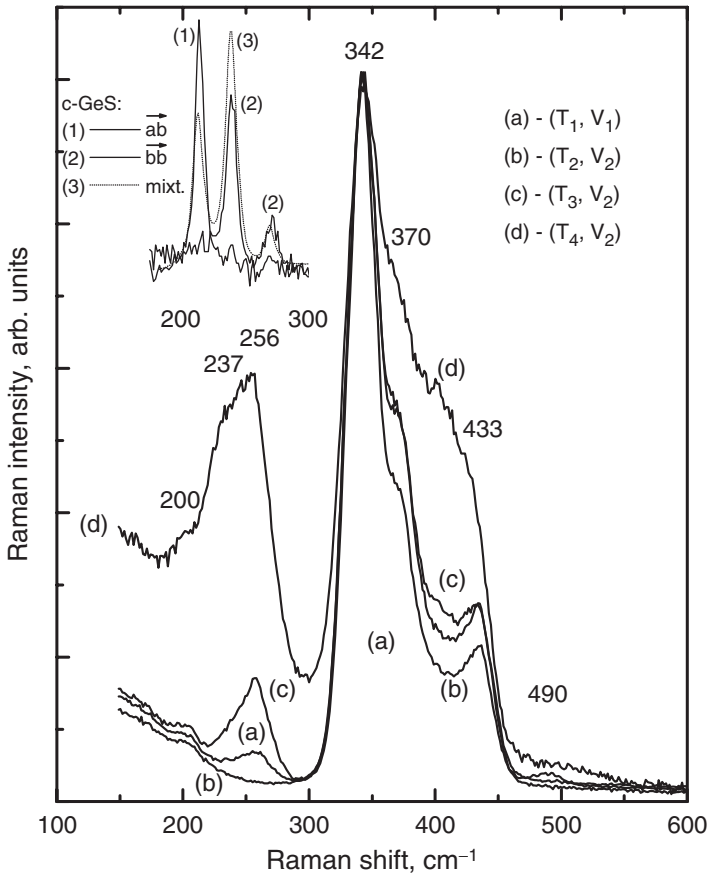

Figure 2. The Raman spectra of g-GeS_2 prepared using different technological conditions and excited by Ar-ion laser beam with wavelength 514.5 nm. All spectra were normalized to the main band at 342 cm^{-1}. Inset shows the Raman spectra of c-GeS measured in $\overrightarrow{ab}$ and $\overrightarrow{bb}$ polarization geometry.

As seen there are many possible contributors to the main features, in the 235–435 cm^{-1} region, and this is also true for the weaker features such as the peak at ~200 cm^{-1}. However, only two clusters ($Ge_3S_{5+4/2}$ and Ge_2S_6 (S–S ends)) contribute above 450 cm^{-1}.

The occupied and unoccupied MO's for the "normally" coordinated (*i.e.* Ge is four- and S is two-fold coordinated) Ge_nS_m clusters are shown in figure 5. However, clusters with tri-coordinated S or Ge ($SGe_{3/3}$, SGe_3–$S_{6/3}$, and $GeS_{3/3}$) represent the local structure of c-GeS better. The charge of these clusters resulted in MO energies shifting and therefore, their MO values were excluded from figure 5. In table 2 the calculated band gaps of Ge_nS_m clusters are shown as obtained both as differences between HOMO and LUMO energies (ΔE_{g1}) and as differences between ground state and first excited state energies (ΔE_{g2}) using TD-DFT. The narrowest band gap, regardless of method, is clearly obtained for the Ge_2S_6 cluster with S–S ends,

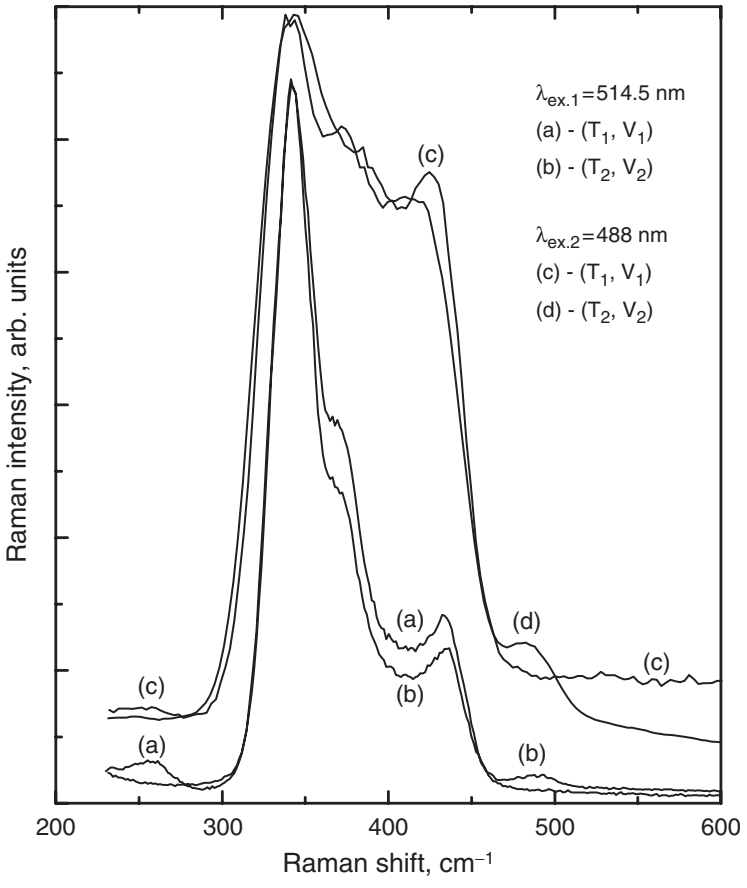

Figure 3. The Raman spectra of (T_1, V_1) (a, c) and (T_2, V_2) (b, d) excited with two different laser beams. All spectra were normalized to the main band at 342 cm^{-1}.

while the other cluster with an S–S connection ($Ge_3S_{5+4/2}$) has a similarly high HOMO, but a higher energy LUMO resulting in a significantly, by about 0.6–0.7 eV, larger band gap.

3.3. *Measured absorption edges of g-GeS_2*

The absorption spectra at 80 and 293 K of the (T_2, V_2) and (T_3, V_2) samples are shown in figure 6 together with the absorption spectrum of c-GeS_2 [25] at 293 K. The energy range shown corresponds to the so-called Urbach tail [26]. Both the position and the slope of the absorption coefficient depend on the glass synthesis conditions (figures 6a and b). We will determine the glassy pseudo band gaps at $\alpha = 10^3\,cm^{-1}$ (generally, the so-called Tauc gap (E_0) of amorphous materials is related to an α level of $5*10^3\,cm^{-1}$ [26]). An energy of 3.05 eV at $\alpha = 10^3\,cm^{-1}$ and 293 K corresponds to the pseudo band gap for (T_2, V_2). For an increased melt temperature sample (T_3, V_2) this value shifts to 3.15 eV. For comparison,

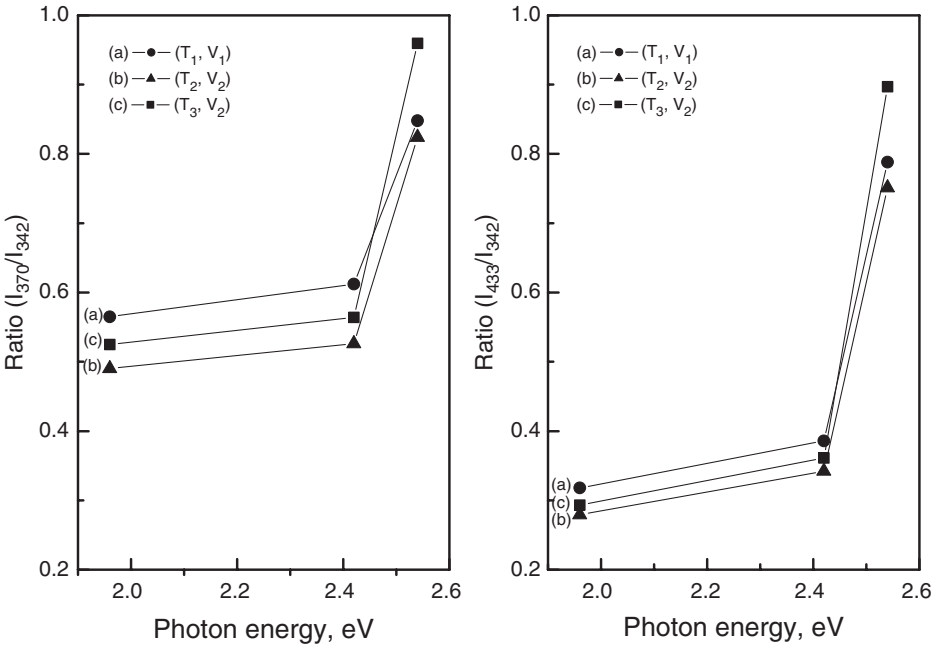

Figure 4. The ratios of the 370 and 433 cm^{-1} Raman intensities relative to the 342 cm^{-1} mode intensity for different excitation photon energies.

the corresponding band gap of c-GeS_2 is larger than 3.4 eV at 293 K. The band gaps become shifted by similar amounts for both glassy samples when the temperature of measurement is lowered to 80 K.

4. Discussion

4.1. *Local structure and Raman spectra of g-GeS_2*

By merging the experimental observations for the g-GeS_2 samples with the computed Raman spectra of various atomic models we aim to propose local structural models for the different glasses investigated. For clarity the two discernible spectral regions: (i) 300–500 cm^{-1} and (ii) 200–300 cm^{-1} (figure 2) are analysed separately.

4.1.1. The spectral region 300–500 cm^{-1}. This region has at least three vibrational modes at ~342, ~370, and ~433 cm^{-1}. The main band at ~342 cm^{-1} has been assigned to A_1-type stretching vibrations in the basic building blocks of this material: single GeS_4 tetrahedra and corner-shared bi-tetrahedra [4]. The strong Raman intensity indicates that these tetrahedra are the main structural units of g-GeS_2. Our calculations support this and show strong modes at 355 cm^{-1} for $GeS_{4/2}$, 342 cm^{-1} for $Ge_2S_{1+6/2}$, 346 and 351 cm^{-1} for $Ge_3S_{3+6/2}$ and $Ge_3S_{5+4/2}$ clusters, respectively (table 1). All these clusters are composed mainly of GeS_4 tetrahedra or bi-tetrahedra.

Table 1. Vibrational frequencies and Raman intensities for the Ge_nS_m clusters (HF/6-311G*).

Cluster	ω* (cm^{-1})	I^R ($Å^4$/a.m.u.)	Cluster	ω* (cm^{-1})	I^R ($Å^4$/a.m.u.)
$GeS_{4/2}$	355	32.4	$SGe_{3/3}$	221	16.2
	409	12.9		291	4.0
	413	10.1		303	3.8
$Ge_2S_{1+6/2}$	342	49.3	SGe_3–$S_{6/3}$	211	12.4
	399	11.1		212	11.0
	408	16.5		217	6.3
	411	5.2		223	10.9
	411	14.4		246	9.9
	415	5.3		274	5.8
	419	15.1			
$Ge_2S_{2+4/2}$	348	6.3	Ge_2S_6	359	5.2
	381	59.9	(S–S ends)	367	41.7
	413	25.4		367	28.1
	441	19.1		443	64.1
				540	98.3
$Ge_2S_{6/2}$	250	25.4	$GeS_{3/3}$	220	11.6
	391	35.0		231	15.6
	396	18.9			
	402	20.9			
	407	5.8			
	409	11.6			
$Ge_3S_{3+6/2}$	347	52.6	$Ge_3S_{5+4/2}$	351	40.2
	399	9.7	(S–S ends)	359	21.4
	406	6.7		401	8.9
	408	17.2		405	12.1
	411	5.7		411	18.5
	414	22.4		415	5.6
	417	8.5		422	11.7
	422	15.2		425	14.7
	425	5.0		431	11.2
				509	15.5

*An empirical scale factor of 0.94 has been applied.

The origins of the two Raman modes at $\sim 370\,cm^{-1}$ (the so-called "companion A_1 Raman mode"- A_1^c) and at $\sim 433\,cm^{-1}$, respectively, are ambiguous at present [27, 28]. Generally, the A_1^c mode has been associated with medium-range order in the glasses, *i.e.* with large "outrigger raft" structures proposed by Phillips *et al.* [4, 29, 30]. However, a more recent interpretation is that of a cluster edge type of mode [12]. There are also at least two interpretations of the mode at $\sim 433\,cm^{-1}$. It is either assigned to edge-shared bi-tetrahedra or to S-dimers, *e.g.* by using the "outrigger raft" Phillips' cluster. The ratios I_{370}/I_{342} and I_{433}/I_{342} can be changed using different excitation wavelengths (figure 3) and the proportional change of the two ratios indicates the common nature of the two peaks (figure 4). Clusters that contribute in this region with large Raman intensity peaks are the $Ge_3S_{5+4/2}$ cluster (with double peaks at 351/359 and 411/425 cm^{-1}) and the $Ge_2S_{2+4/2}$ cluster (with peaks at 381 and 413 cm^{-1}). The former cluster has an S–S bond, while the latter

Figure 5. The energies of occupied and unoccupied MO's for the Ge_nS_m clusters (BLYP/6-311G*).

Table 2. Calculated band gaps of the Ge_nS_m clusters by using differences in HOMO and LUMO energies (ΔE_{g1}) (BLYP/6-311G*) and differences in ground and first excited states energies (ΔE_{g2}) (TD-BLYP/6-311G*).

Cluster	ΔE_{g1} (eV)	ΔE_{g2} (eV)	Cluster	ΔE_{g1} (eV)	ΔE_{g2} (eV)
$GeS_{4/2}$	3.43	3.60	$SGe_{3/3}$	2.72	2.89
$Ge_2S_{1+6/2}$	3.15	3.23	SGe_3–$S_{6/3}$	2.89	3.08
$Ge_2S_{6/2}$	2.87	3.20	$GeS_{3/3}$	3.96	4.46
$Ge_2S_{2+4/2}$	2.99	3.08	Ge_2S_6 (S–S ends)	1.71	1.74
$Ge_3S_{3+6/2}$	2.97	3.01	$Ge_3S_{5+4/2}$ (S–S ends)	2.31	2.43

is a cluster that may indicate that these modes can be attributed to edge-sharing GeS_4 tetrahedra. To resolve this issue we note the changed ratios of the modes with different excitation wavelengths, to be discussed further in the next section.

As for the role of the technological conditions of synthesis only, the (T_2, V_2) sample has a very weak feature at $\sim$490 cm^{-1}, but on the other hand no other strong peaks than the three typical modes. Among the different glasses this sample also results in the relatively weakest 370 and 433 cm^{-1} peaks. Accordingly, the ratios I_{370}/I_{342} and I_{433}/I_{342} are smallest for (T_2, V_2), a behaviour preserved for different photon energies (figure 4), as all glasses follow the same trend with respect to changed wavelengths of excitation. However, the feature at $\sim$490 cm^{-1} is important as the only cluster that provides us with a calculated feature in the vicinity is $Ge_3S_{5+4/2}$ with a mode at 509 cm^{-1}. Thus, the presence of S–S bonds and their contribution to this region overall is supported, but only for the (T_2, V_2) sample, while for all other

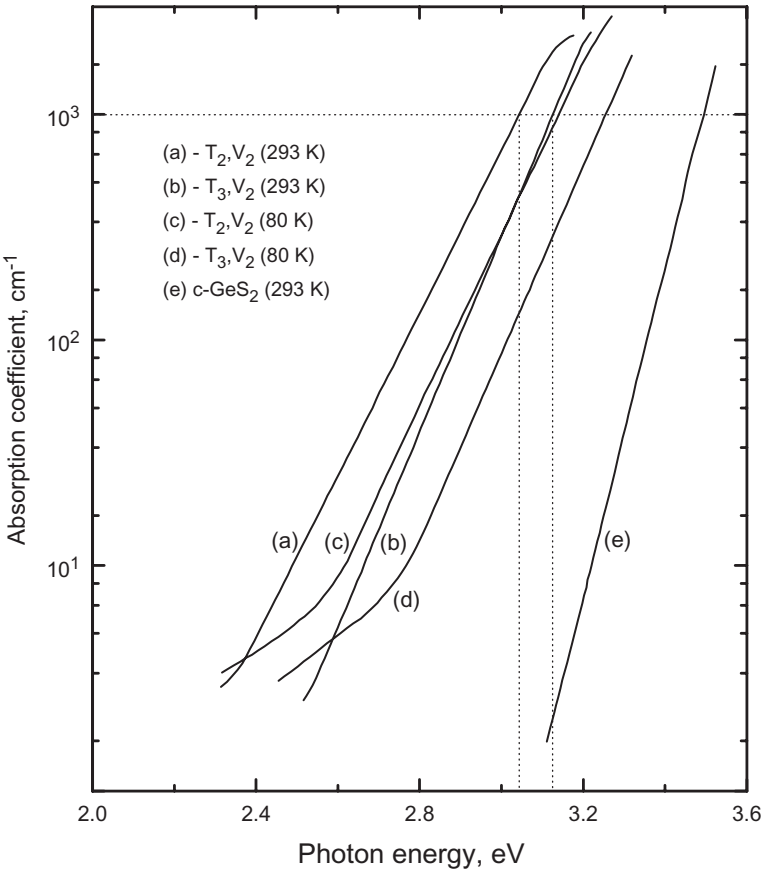

Figure 6. The absorption coefficients (α) of the GeS_2 glasses at 293 and 80 K: (a, c) (T_2, V_2) and (b, d) (T_3, V_2). The absorption edge of c-GeS_2 (e) [25] shown for comparison.

samples edge-shared tetrahedra is the suggested structural basis for the observed peaks.

4.1.2. The spectral region 200–300 cm^{-1}. This spectral region shows a main feature at $\sim$256 cm^{-1} (figure 2), which had previously been assigned to the presence of ethane-like structural units with Ge–Ge bonds within the glass matrix [31]. This band is highly sensitive to the preparation conditions and absent for (T_2, V_2) while second in strength in the entire spectra of (T_4, V_2). Together with this peak, a shoulder at $\sim$237 cm^{-1} also develops. The experimental peaks at 256 cm^{-1} correlate with the calculated Ge-Ge stretching mode in the ethane-like $Ge_2S_{6/2}$ cluster (250 cm^{-1}) or the mode calculated at 246 cm^{-1} obtained for SGe_3–$S_{6/3}$. However, the shoulder at $\sim$237 cm^{-1} can only be related to the formation of new structural units all having tri-coordinated S or Ge ($SGe_{3/3}$, SGe_3–$S_{6/3}$, and $GeS_{3/3}$) as no other clusters have any peaks below 250 cm^{-1}. The band near 237 cm^{-1} is a breathing-like A_g mode [32] in the polarized spectra of c-GeS for $\vec{b}\vec{b}$ polarization. It is known

that the basic building block of c-GeS is a pyramid where both S and Ge atoms are three-fold coordinated. It is thus tempting to ascribe both features to SGe_3–$S_{6/3}$ units, and thus with no Ge–Ge bonds at all present in the materials, or possibly in combination with $Ge_2S_{6/2}$ units. Previously, homo-polar bonds (Ge–Ge) in g-GeS_2 have not been detected by neutron experiments [33], but this has been ascribed to the sensitivity limit of a diffraction measurement [34]. Moreover, interpretation of the 256 cm^{-1} mode as a breathing-type vibration of distorted rocksalt GeS microphase has also been made [4].

The very weak band detected at ~200 cm^{-1} is in accordance with our calculated Raman peaks at 211 and 212 cm^{-1} for the SGe_3-$S_{6/3}$ cluster that in turn are in excellent accordance with the 212 cm^{-1} B_{3g} mode for c-GeS [32]. For small c-GeS clusters implanted into pores of zeolites (X-GeS) this peak is located near ~200 cm^{-1} and is the dominant peak (figure 1, Ref. [15]). Accordingly, the calculated Raman peaks for the SGe_3–$S_{6/3}$ cluster indicate the dominant mode in the integrated Raman spectrum. Therefore, c-GeS nano-particles with sizes about 7–12 Å [15] may exist in the (T_2, V_2) glass structure. Other synthesis conditions than (T_2, V_2) may result in association of these clusters and the formation of larger c-GeS particles within the matrix of g-GeS_2.

Altogether the non-resonant Raman results combined with the *ab initio* calculations support the co-existence of single GeS_4 tetrahedra, corner-shared and edge-sharing GeS_4 tetrahedra together with tri-coordinated S or Ge ($SGe_{3/3}$, SGe_3–$S_{6/3}$, and $GeS_{3/3}$). For the (T_2, V_2) sample also a S–S bond containing $Ge_3S_{5+4/2}$ cluster contributes to a very minor extent.

4.2. *Band gaps and absorption edges of g-GeS_2*

The short-range order was shown above to be different for the samples and consequently we believe that the optical gap of g-GeS_2 can be modified using different conditions of preparation. Sulfur atoms are known to form the basis of the valence band of germanium disulfide by lone-pair electron states [26]. The lone pair electrons interact through the π-orbitals [23]. In edge-shared tetrahedra the sulfur atoms are in a strained state in comparison with corner-shared tetrahedra. The interaction of such sulfur atoms can produce electronic states near the top of the valence band. In figure 5 the MO's of Ge_nS_m clusters are shown. The HOMO energy values of most Ge_nS_m clusters are all close to −6.3 eV. However, the $Ge_3S_{5+4/2}$ cluster has a higher lying HOMO (−5.8 eV). This is due to the S–S bonds being present. This cluster is, however, in general considered less likely in light of the results above. For the (T_2, V_2) sample, however, the observed increase of the 490 cm^{-1} mode with a higher exciting photon energy (figure 3) supports the existence of the $Ge_3S_{5+4/2}$ cluster.

In general, the edge-shared $Ge_2S_{2+4/2}$ cluster is considered more likely to contribute to the resonant Raman spectra in figure 3, but has a much larger band gap than 2.54 eV (2.99–3.08 eV, table 2). However, by closing the structure, modifying the $Ge_2S_{2+4/2}$ cluster (S–S distance ~3.43 Å) to the Ge_2S_6 (S–S ends) cluster (~2.31 Å), both the HOMO changes upward (−5.8 eV) and the band gap becomes much smaller than 2.54 eV (1.71–1.74 eV). Thus small variations in the local structure seem to be able to be responsible for both the Raman spectra (as provided

by the edge-shared $Ge_2S_{2+4/2}$ cluster) and the resonant Raman spectra (as provided by the closed Ge_2S_6 (S–S ends) cluster. Therefore, we conclude that S–S bonds form the band tail states at the top of the valence band of g-GeS_2, a result in accordance with the results of electronic density of states (DOS) calculated by Louie [13] for g-$GeSe_2$.

In figure 6 we show the absorption edge measurement results for (T_2, V_2) and (T_3, V_2) at room and liquid nitrogen temperatures and in addition c-GeS_2 [25] for comparison. The absorption coefficient of (T_2, V_2) at $\alpha = 10^3\,cm^{-1}$ corresponds to a band gap of 3.05 eV. Calculated gaps of $Ge_2S_{1+6/2}$ and $Ge_2S_{2+4/2}$ are 3.15–3.23 eV and 2.99–3.08 eV, respectively. On the other hand, if the $Ge_3S_{5+4/2}$ cluster would contribute the band gap should be much lower (calc. 2.43 eV). This hardly indicates that this Philips "outrigger raft" cluster realizes in the structure of the glass to any large extent, as also seen by the very weak intensity of the $490\,cm^{-1}$ band as discussed above.

The absorption edge of g-GeS_2 shifts and corresponds to an optical gap of 3.15 eV for (T_3, V_2), a value still possible to ascribe to $Ge_2S_{1+6/2}$ or $Ge_2S_{2+4/2}$ clusters. The corner- and edge-shared clusters have a delicate balance as previously calculated from formation energies of $Ge_2S_{1+6/2}$ and $Ge_2S_{2+4/2}$ clusters [35], and the up-shifted absorption edge is possibly due to concentration differences among the two clusters. This shift can also be related to the absence of S–S bonds in the structure of (T_3, V_2) sample in comparison with (T_2, V_2). The role of three-fold coordinated SGe_3–$S_{6/3}$ cluster (2.89–3.08) is still negligible here.

The absorption edge of (T_4, V_2) is not shown in figure 6 as the thickness of the sample did not provide the maximum accuracy, but crude results provide a red-shift and hence an optical gap less than 3.05 eV. The decreased gap can only occur by association of three-fold coordinated $SGe_{3/3}$ clusters and formation of c-GeS micro-phases (room temperature optical energy gap of 1.57 eV was measured for the $\vec{b}$ axis of c-GeS [36]), in excellent accordance with the results of Raman spectra in the 200–300 cm^{-1} region.

5. Conclusions

The combined picture of the local structure of the g-GeS_2 samples is as follows:

(i) All glasses contain corner-shared and edge-shared GeS_4 tetrahedra. With increased melt temperature or reduced cooling rate the amount of edge-shared GeS_4 tetrahedra and tri-coordinated S or Ge structures increases. The SGe_3–$S_{6/3}$ is the local structure that we found to compare most favorably with the collection of experimental data. Even the second lowest melt temperature and fastest cooling rate sample, (T_2, V_2), has a detectable amount of the SGe_3–$S_{6/3}$ tri-coordinate structures in addition to the $Ge_3S_{5+4/2}$ S–S bond containing cluster.

(ii) The common nature of the features at 370 and $433\,cm^{-1}$ as seen in the resonance Raman measurements together with the non-resonant Raman peak positions allow us to assign both these peaks to originate in $Ge_2S_{2+4/2}$ clusters.

(iii) The origin of the band gaps of g-GeS_2 is very complex, but nevertheless the results allow us to conclude that the formation of S–S bond(s) lead to the

creation of a localized state near the top of the valence band. A delicate balance of different S–S distances within the glasses seems to determine the exact value of the band gap observed. Further decreased band gaps are obtained for the (T_4, V_2) sample resulting from the extensive formation of tri-coordinate structures, which can be similar to a c-GeS micro-phase. It is thus possible to modulate the band gaps by the synthesis procedure, both by melt temperature and by cooling rate.

(iv) There is no support for the existence of Ge–Ge bonds in any of the glasses.

Acknowledgements

We are grateful to N. Mateleshko for many helpful discussions and M. Veresh (Hungarian Institute for Solid State Physics and Optics) for his assistance in part of the experiments. R.H. would like to thank the Swedish Institute for scholarship support. The present work was partially supported by the ministry of education and science of Ukraine (Grant Nos. M/467-2003 and 29/48-2001). The main part of the calculations was performed at the Condensed Matter Physics Group (CTH) Linux cluster.

References

[1] P.H. Gaskell, in *Proceedings of the Sixth International Conference on the structure of Non-Crystalline Materials (NCM6)*, Prague, Czech Republic, edited by L. Cervinka and A.C. Wright (Netherlands: North-Holland; 1995), p. 9.
[2] I. Fekeshgazi, K. May, V. Mitsa and A. Vakaruk, *Physics and Applications of Non-Crystalline Semiconductors in Optoelectronics*, edited by A. Andriesh and M. Bertolotti (Kluwer Academic Publishers, Dordrecht/Boston/London, 1997), Vol. 36, p. 243.
[3] E. Robinel, B. Carette and M. Ribes, J. Non-Cryst. Solids **57** 49 (1983).
[4] P. Boolchand, J. Grothaus, M. Tenhover, M.A. Hazle and R.K. Grasselli, Phys. Rev. B **3** 5421 (1986).
[5] A. Perakis, I.P. Kotsalas, E.A. Pavlatou and C. Rapris, Phys. Stat. Sol. (B) **211** 421 (1999).
[6] Z. Cernosek, E. Cernoskova and L. Benes, J. Mol. Structure **435** 193 (1997).
[7] N. Mateleshko, V. Mitsa and R. Holomb, Physica B **349** 30 (2004).
[8] K. Tanaka and M. Yamaguchi, J. Non-Cryst. Solids **227–230** 757 (1998).
[9] X. Zhao, H. Higuchi and Y. Kawamoto, Phys Chem. Glasses **39** 98 (1998).
[10] S. Blaineau, P. Jund and D. Drabold, Phys. Rev. B **67** 094204 (2003).
[11] S. Blaineau and P. Jund, Phys. Rev. B **69** 064201 (2004).
[12] K. Jackson, A. Briley, S. Grossman, D.V. Porezag and M.R. Pederson, Phys. Rev. B **60** R14985 (1999).
[13] S. Louie, Phys. Rev. B **26** 5993 (1992).
[14] V.M. Mitsa, *Vibrational spectra and structural correlation in non-oxide glassy alloys*, edited by Ya. M. Valakh and V.S. Gerasimenko (UMK VO: Kiev, 1992).
[15] I. Fejsa, V. Mitsa and D. Bletskan, J. Mol. Structure **480–481** 695 (1999).
[16] M.J. Frisch, G.W. Trucks, H.B. Schlegel, G.E. Scuseria, M.A. Robb, *et al.*, Gaussian, Inc., Pittsburgh PA, 2003.
[17] V.A. Rassolov, J.A. Pople, M.A. Ratner and T.L. Windus, J. Chem. Phys. **109** 1223 (1998).

[18] M.W. Schmidt, K.K. Baldridge, J.A. Boatz, S.T. Elbert, M.S. Gordon, M. S., J.J. Jensen, S. Koseki, N. Matsunaga, K.A. Nguyen, S. Su, T.L. Windus and M. Dupuis, J. Comput. Chem. **14** 1347 (1993).
[19] R. Holomb and V. Mitsa, Solid State Commun. **129** 655 (2004).
[20] R. Holomb, P. Johansson and V. Mitsa, Submitted to *Phys. Rev. B* (2004).
[21] A.D. Becke, Phys. Rev. A **38** 3098 (1998).
[22] C. Lee, W. Yang and R.G. Parr, Phys. Rev. B **37** 785 (1998).
[23] R. Stowasser and R. Hoffmann, J. Am. Chem. Soc. **121** 3414 (1999).
[24] R.E. Stratmann, G.E. Scuseria and M.J. Frisch, J. Chem. Phys. **109** 8218 (1998).
[25] D.I. Bletskan, *Crystalline and Glassy Chalcogenides Si, Ge, Sn and Alloys Based on Them: Monograph* (Uzhgorod: Transcarpathia, 2004).
[26] N.F. Mott and E.A. Davis, *Electronic Processes in Non-Crystalline Materials*, 2nd edn (Clarendon Press: Oxford, 1979).
[27] K. Inoue, O. Matsuda and K. Murase, J. Non-Cryst. Solids **150** 197 (1992).
[28] M. Gobb, D.A. Drabold and R.L. Cappalletti, Phys. Rev. B **54** 12162 (1996).
[29] J.A. Aronovitz, J.R. Banavar, M.A. Marcus and J.C. Phillips, Phys. Rev. B **28** 4454 (1983).
[30] P.M. Bridenbaugh, G.P. Espinosa, J.E. Griffiths, J.C. Phillips and J.P. Remeika, Phys. Rev. B **20** 4140 (1979).
[31] G. Lucovsky, R.J. Nemanich and F.L. Galeener, in *Proceedings of the Seventh International Conference on Amorphous and Liquid Semiconductors,* Edinburgh, Scotland, edited by W.E. Spear (Dundee: G.G. Stevenson; 1977), p. 130.
[32] J.D. Wiley, W.J. Buckel and R.L. Schmidt, Phys. Rev. B **13** 2489 (1976).
[33] I. Petri and P.S. Salmon, J. Non-Cryst. Solids **293–295** 169 (2001).
[34] C. Liuchun and P. Boolchand, Phil. Mag. B **82** 1649 (2002).
[35] R.M. Holomb, J. Physics and Chemistry of Solid State **4** 711 (2003) (in Ukrainian).
[36] A.M. Elkorashy, J. Phys. C: Solid State Phys. **21** 2595 (1988).